Biophysical Chemistry 159 (2011) 275–286

Contents lists available at ScienceDirect

Biophysical Chemistry

journal homepage: http://www.elsevier.com/locate/biophyschem

Molecular dynamics simulations of T-20 HIV fusion inhibitor interacting with model membranes

A.M.T. Martins do Canto [a,b], A.J. Palace Carvalho [a,b], J.P. Prates Ramalho [a,b], Luís M.S. Loura [c,d,*]

[a] Departamento de Química, Universidade de Évora, Portugal
[b] Centro de Química de Évora, Universidade de Évora, Portugal
[c] Faculdade de Farmácia, Universidade de Coimbra, Portugal
[d] Centro de Química de Coimbra, Universidade de Coimbra, Portugal

HIGHLIGHTS

- ▶ HIV fusion inhibitor T-20 (enfuvirtide) was studied by molecular dynamics simulations.
- ▶ The inhibitor peptide was simulated in both POPC and POPC/Cholesterol 1:1 bilayers.
- ▶ T-20 showed a more limited extent of interaction with model membranes than T-1249.
- ▶ Interaction with POPC/Cholesterol bilayers is especially weak, no penetration occurs.
- ▶ The weaker interaction with membranes correlates with a smaller inhibitory efficiency.

GRAPHICAL ABSTRACT

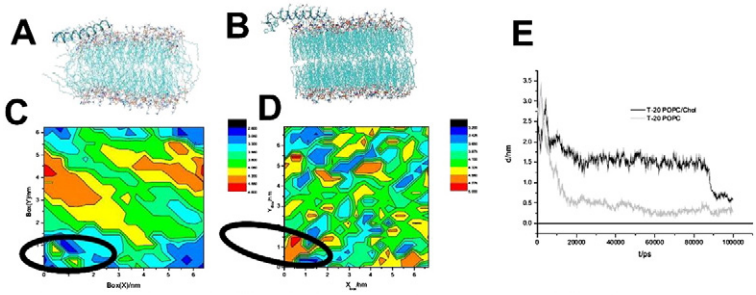

(A) and (B) Final structure snapshots of the T-20 peptide with the model membranes in this study, POPC and POPC/Chol, respectively.
(C) and (D) Final structure membrane thickness as a function of XY box dimensions. Peptide position is highlighted as a black ellipse.
(E) Timecourse of the distance between the peptide center of mass and the bilayer surface.

ARTICLE INFO

Article history:
Received 3 May 2011
Received in revised form 31 July 2011
Accepted 1 August 2011
Available online 6 August 2011

Keywords:
AIDS
HIV fusion inhibitor
Lipid bilayer
Enfuvirtide
Lipid–peptide interaction
Molecular dynamics

ABSTRACT

T-20 (also known as enfuvirtide) is a fusion inhibitor peptide known to have some effectiveness in the control of progression of HIV infection by inhibiting the fusion of the HIV envelope with the target cell membrane. Recent results indicate that T-20 is able to interact with membranes in the liquid disordered state but not with membranes in an ordered state, which could be linked to its effectiveness. A detailed molecular picture of the interaction of these molecules with membranes is still lacking. To this effect, extensive molecular dynamics simulations (100 ns) were carried out to investigate the interaction between T-20 and bilayers of 1-palmitoyl-2-oleoyl-phosphatidylcholine (POPC) and POPC/cholesterol (1:1). Membrane properties such as area/lipid, density profiles, order parameters and membrane thickness were studied. It was observed that T-20 has the ability to interact to different extents with both model membranes in this study and that peptide interaction with the bilayer surface has a local effect on membrane structure. The formation of hydrogen bonding between certain peptide residues and the POPC phosphate group was observed. However, T-20 showed a more limited extent of interaction with model membranes when compared with other, more efficient, peptides (such as T-1249). This effect is most notable in POPC/Chol membranes in which interaction is especially weak, owing to less peptide residues acting as H bond donors to POPC and virtually no H bonds being formed between T-20 and cholesterol. This lower ability to interact with membranes is probably correlated with its smaller inhibitory efficiency.

* Corresponding author at: Faculdade de Farmácia, Universidade de Coimbra, Pólo das Ciências da Saúde, Azinhaga de Santa Comba, 3000-548 Coimbra, Portugal. Tel.: +351 239488485; fax: +351 239827126.
E-mail address: lloura@ff.uc.pt (L.M.S. Loura).

0301-4622/$ – see front matter © 2011 Elsevier B.V. All rights reserved.
doi:10.1016/j.bpc.2011.08.001

1. Introduction

Binding of the HIV virus to the target cell and fusion of the membranes of both (initial steps of HIV infection) are mediated by the viral glycoprotein complex formed by the transmembrane protein gp41, and the surface protein gp120, bound to the external domain of gp41 [1]. This is an obligatory process of viral infection. Entry of HIV into a target cell is performed in three steps: (i) binding of the viral gp120 to the target cell surface protein CD4 [2]; (ii) conformation change of gp120 enabling this protein to bind to yet another receptor on the immune system cell's surface, typically CCR5 [3] or CXCR4 [4]; and (iii) gp41-mediated membrane fusion [1].

Several peptides based on the C-region of HIV's gp41 have been used in clinical trials as possible HIV fusion inhibitors (reviewed in [5]). Among these is T-20. T-20 or enfuvirtide is a HIV entry inhibitor approved for clinical use [6]. It is a 36-amino-acid peptide, homologous to the C-terminal region of HR2 of HIV-1 gp41 [7–10]. The elucidation of the core structure of gp41 has helped to understand the inhibitory activity of enfuvirtide [9]. The peptide sequence (sequence 643–678 of HIV-1_{LAI}[7]) corresponded partially to the CHR region of gp41 and it would bind to the opposite NHR region, preventing the formation of the hairpin structure and consequently, the fusion. Despite the therapeutic potency of enfuvirtide, it has met the emergence of resistant strains.

Similar peptides have been synthesized in order to achieve fusion inhibition without this setback. Among these T-1249 stands out. T-1249 is a 39-aminoacid fusion inhibitor peptide, composed of sequences derived from HIV-1, HIV-2, and simian immuno-deficiency virus (SIV) [11]. Initial clinical trials with T-1249 have shown promising results; namely, it is a more potent inhibitor than T-20 even with a single daily administration instead of the two used for enfuvirtide and retains activity against most enfuvirtide-resistant strains [7,9,11,12].

The differences in the effectiveness of these peptides are still a matter of debate and a detailed molecular picture of the inhibitory mechanism promoted by these fusion inhibitors is still incomplete. Both T-20 and T-1249 showed an efficient partition to zwitterionic bilayers, however only T-1249 is able to interact/adsorb effectively to cholesterol-rich membranes, which may be the main cause of its improved efficiency (see [13,14] for a detailed discussion). Both fluorescence spectroscopy data [13,14] and simulation [15] studies have shown the capacity these peptides have to adsorb/interact to the bilayer surface and suggest this as at least part of its mechanism of action.

In this work, we study the interaction of T-20 with 1-palmitoyl-2-oleoyl-phosphatidylcholine (POPC) and POPC/cholesterol (Chol) membranes using molecular dynamics (MD) simulations in the 100 ns time scale. It is concluded that the peptide adsorbs (with less affinity than T-1249) to the surface of both bilayers (weakly in the POPC/Chol bilayer), without insertion in the studied timescale. T-20 presents a helical structure, which has been related in the literature to increased efficiency in HIV fusion inhibition. The peptide diffuses in the plane of the bilayer and possesses limited rotational freedom. These observations mostly agree with the model of Veiga et al. [13] for the role of lipid bilayers in the mode of action of the peptide and may explain the relative poor action of T-20 against HIV fusion when compared with other similar peptides [16], since low affinity to the bilayers implies low local concentrations of the inhibitor and thus the bilayer surface is not able to act efficiently as a reservoir for the anti-fusion peptide.

2. Simulation and analysis details

The initial α-helix model of T-20 (see Fig. 1A for primary structure) was built with the Arguslab 4.01 package [17] and solvated in a cubic simulation box with SPC water [18], allowing for a distance between peptide and the box walls of 0.5 nm. POPC model molecules (Fig. 1B) and their bonded and non-bonded parameters were downloaded from the Tieleman group web page (http://moose.bio.ucalgary.ca/index.php?page=Structures_and_Topologies). Cholesterol model molecules (Fig. 1C) and their bonded and non-bonded parameters were taken from [19] and were downloaded from the GROMACS web page (http://www.gromacs.org/index.php?title=Download_%26_Installation/User_contributions/Molecule_topologies). Initial models of both membranes (POPC, 126 molecules; and POPC/Chol (1:1), 240 molecules in total; see Fig. 1) were built. To this purpose, one POPC molecule (with mostly stretched and parallel acyl chains) from the downloaded POPC bilayer pdb file (together with one Chol molecule in the case of the POPC/Chol system) was replicated to build custom size model bilayers using GROMACS model preparation packages [20,21]. The latter was also used to perform all simulations. The GROMACS force field (which is a modified GROMOS87 force field) was used to describe all the interactions (see the GROMACS manual for details, ftp://ftp.gromacs.org/pub/manual/manual-3.3.pdf). Molecular dynamics of these systems, under the same conditions as the final MD runs (see below), were performed for at least 50 ns to ensure that the bilayers were equilibrated prior to the peptide inclusion in the system, losing memory of their initial structure in the process. Peptide and bilayer models were then combined, and the final structure obtained after 100 ns simulation of T-20 in water was used as the initial structure of the simulations of the peptide interacting with the bilayer systems. The zz dimension of the simulation box was increased for this purpose, and the peptide molecule was positioned, with the helix's axis parallel to the bilayer surface (but with otherwise random orientation of its residues relative to the bilayer), at about 2.7–2.9 nm above the average position of the lipid P atoms of the top leaflet. The number of added SPC water molecules was sufficient to ensure full peptide and bilayer hydration in all systems (9243 water molecules added to the POPC bilayer system – with average dimensions of $6.4\times6.2\times11.1$ nm^3 – and 7057 water molecules added to the POPC/Chol bilayer system — with average dimensions of $6.7\times6.9\times9.2$ nm^3). Systems with no added peptide were also simulated, and the main structural lipid properties were successfully verified for validation purposes, as described below. Prior to the production MD simulation, all systems underwent a steepest-descent energy minimization of the structure followed by a small MD run to properly allow the solvent molecules to adjust/relax around the peptide or membrane. Extensive MD simulations were then performed under constant number of particles, pressure (1 bar) and temperature (300 K), and using periodic boundary conditions. Pressure and temperature control was carried out using the weak-coupling Berendsen schemes [22], with coupling times of 1.0 ps and 0.1 ps, respectively. Isotropic pressure coupling was used for the T-20 simulation in water and semiisotropic pressure coupling was used in all other simulations. All bonds were constrained to their equilibrium values using the SETTLE algorithm [23] for water and the LINCS algorithm [24] for all other bonds. Although our description of POPC is based on a united-atom model, both the peptide and cholesterol contain explicit H atoms. Very fast vibrations involving H atoms require the use of very small integration time steps, and therefore affect the efficiency of MD simulations. Constraining bond lengths allow the use of longer time steps, therefore improving efficiency [25].

The systems were simulated for 100 ns, with a time step of 2 fs. The long-range electrostatic interactions were calculated by the particle-mesh Ewald (PME) summation method [26]. A cut-off of 1.0 nm was used for both van der Waals and the PME direct-space component of electrostatic interactions. Analyses were carried out, mostly, using the GROMACS 3.3.3 analysis package [19,20] with the exception of the peptide secondary structure analysis which was performed with the DSSP package [27] and some membrane thickness calculations that were performed with the GridMat-MD program [28]. Errors were calculated according to the block method of Flyvbjerg and

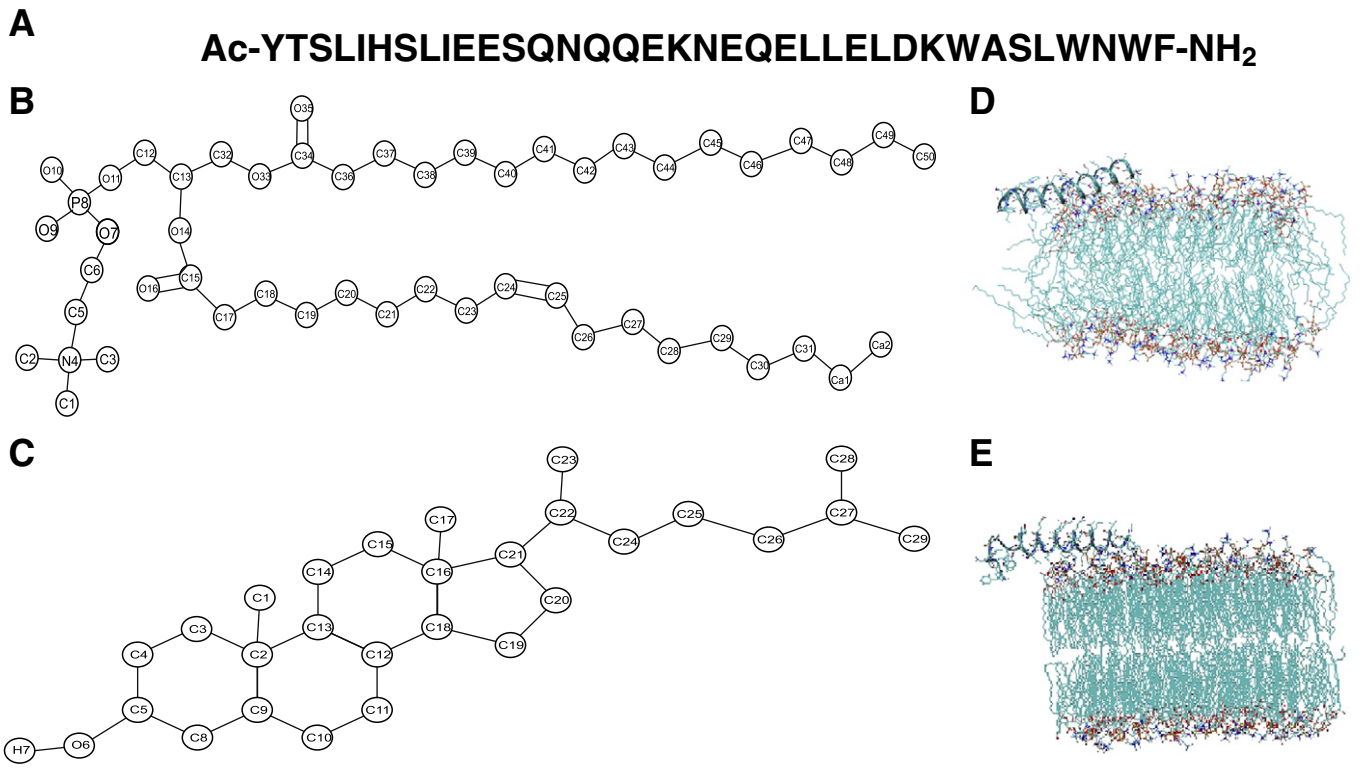

Fig. 1. (A) T-20 aminoacid sequence. (B) POPC structure and atom numbering. (C) Cholesterol structure and atom numbering. (D) T-20/POPC final structure snapshot. (E) T-20/POPC/Chol final structure snapshot.

Petersen [29], except for the diffusion coefficients, whose errors were estimated by calculating the difference between the values calculated from the two halves of the sampling interval.

3. Results

3.1. Equilibration of the membrane system

To evaluate the process of the systems' equilibration, time profiles of the surface area/POPC (Fig. 2A) and surface area/Chol (Fig. 2B) were calculated as described in [30] (Eqs. (1) and (2)) and recorded for the production simulation (100 ns; see section Cross-sectional area per lipid and membrane thickness for a detailed analysis of area/molecule values):

$$A_{POPC} = \frac{2A_{box}}{V_{box} - N_W V_W} \left[\frac{V_{box} - N_W V_W - xN_{lipid} V_{Chol} - V_{T-20}}{(1-x)N_{lipid}} \right] \quad (1)$$

$$A_{Chol} = \frac{2A_{box} V_{Chol}}{V_{box} - N_W V_W - V_{T-20}}. \quad (2)$$

In these equations, A_{POPC} is the cross-sectional area per POPC molecule, A_{Chol} is the cross-sectional area per Chol molecule, A_{box} is the area of xy plane of the simulation box, V_{box} is the simulation box total volume, N_w is the number of water molecules, V_w is the volume of the water molecule (0.0312 nm^3) [30], x = 0.00 or 0.50 is the Chol mole fraction, N_{lipid} is the number of lipid molecules, V_{chol} is the volume of the Chol molecule (0.593 nm^3) [30], and $V_{T\text{-}20} = 16.34$ nm^3 is the volume of the T-20 molecule, determined from the T-20 simulation in water by averaging $V_{T\text{-}20} = V_{box} - N_w \times V_w$ for the last 25 ns of the simulation.

The surface area per lipid is a slowly converging parameter of MD simulation, but its average value was stable over the final 80 ns of the simulation, which led us to the conclusion that the simulated systems had reached a steady state after 20 ns of simulation. One important exception to this fact was the T-20 simulation with the POPC/Chol bilayer. For this system, it was verified that the peptide interacts with the bilayer via the C-terminus for most of the simulation time but only adsorbs completely after 85 ns of simulation (see following section). To take this difference into account, when it was relevant, parameters were analyzed also averaging only for the last 10 ns of the simulation.

3.2. Peptide location and orientation

The positions of the peptide, individual aminoacid residues and terminals were followed by determining their centers of mass coordinates with respect to the bilayer normal direction (*Z*). In the starting configuration, T-20 was placed at approximately 2.7–2.9 nm above the membrane surface, defined as the average of the *Z* positions of all POPC P atoms of the top bilayer leaflet. The closest distances between atoms of T-20 and POPC (1.58 nm and 1.14 nm in the POPC and POPC/Chol systems, respectively) were chosen to be larger than the cutoffs used in the simulations for both van der Waals and the PME direct-space component of electrostatic interactions. T-20 has been characterized as an amphipathic peptide, with one face of the helix displaying a higher capability to interact with the solvent, and the opposite face characterized by a higher capability to interact with the bilayer [31–33]. Nevertheless, because of the large mobility of the peptide in solution (see peptide dynamics section below), the orientation of the two faces of the helix relative to the bilayer in the initial structure was random, still allowing the peptide to adopt a favorable configuration for interaction with the bilayer prior to adsorption. In both membrane systems the peptide approaches, to different extents, the membrane surface in <25 ns (Fig. 2C). In the POPC bilayer system, the peptide adsorbs to the membrane surface and maintains that interaction throughout the rest of the simulation time (Fig. 2C), whereas in the POPC/Chol bilayer system only the C-terminus adsorbs to the bilayer surface during

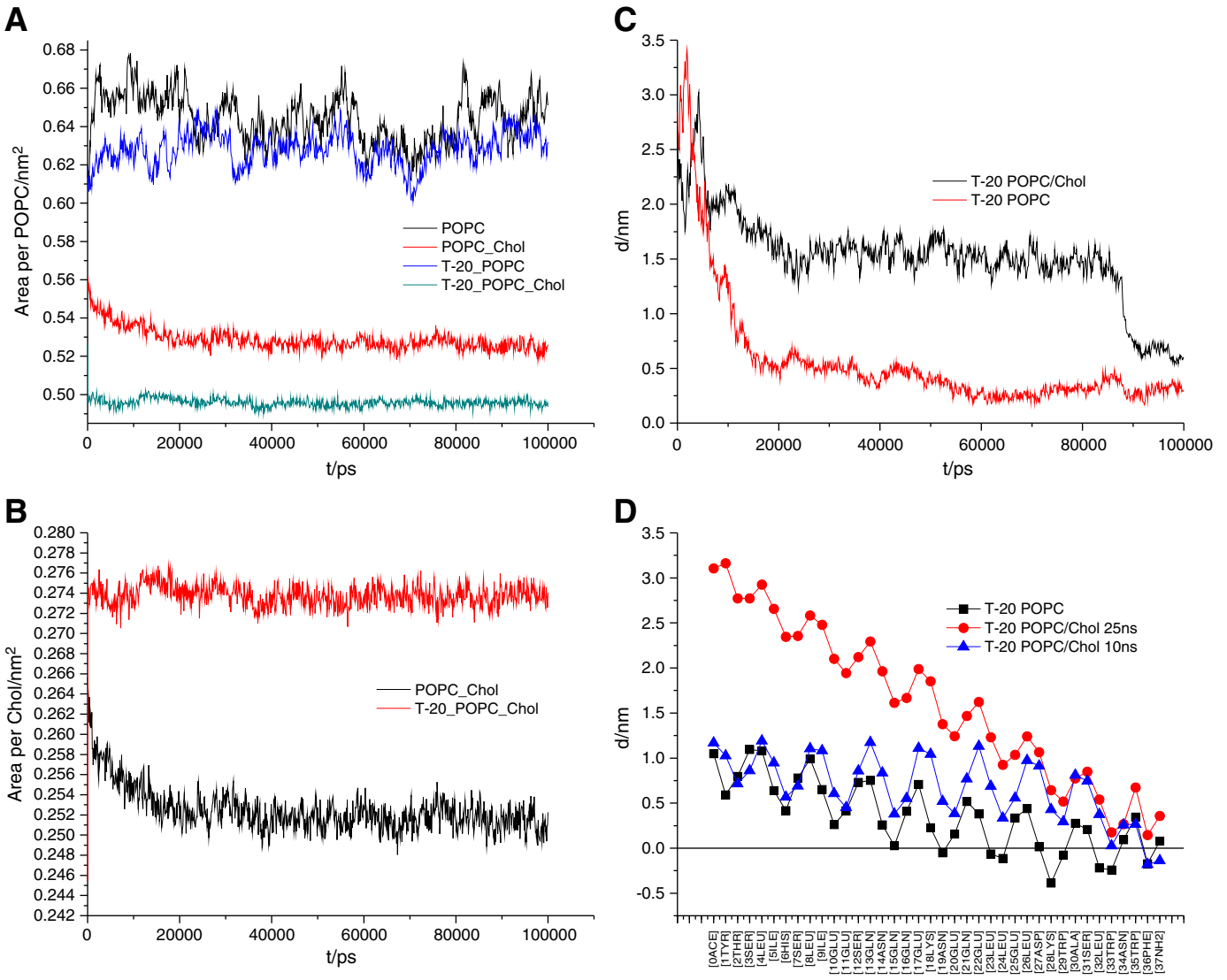

Fig. 2. (A) Area per POPC time course. (B) Area per Chol time course. (C) Time course of T-20's center of mass distance to bilayer surface defined as average Z position of all P atoms. (D) T-20's individual residues' distances to bilayer surface defined as average Z position of all P atoms. Position of each residue was averaged over the last 25 ns of the simulation (both systems) and over the last 10 ns (POPC/Chol system).

approximately the first 85 ns of the simulation (Figs. 2D and 1E). After this, the peptide adsorbs to the bilayer surface similarly to the POPC system (Fig. 2C). Unlike the previously studied peptide, T-1249 [15], T-20 in its equilibrium adsorbed position is not parallel to the membrane surface; in fact, in both simulated systems it displays a tilt (defined as the time average of the angle between the vector defined by the 2nd and 35th Cα and the plane parallel to the membrane surface) of $48° \pm 2°$ and $8° \pm 1°$ for 75–85 ns and the last 10 ns of the simulation, respectively, in the POPC/Chol bilayer system. For the POPC system, the calculated tilt was $18° \pm 2°$. The POPC bilayer is in the liquid disordered state, with increased free volume relative to the POPC/Chol liquid ordered membrane. This is probably related to the increased ability of T-20's C-terminus to penetrate below the average location of POPC's P atoms, as apparent from the average positions of residues Leu 23, Leu 24, Lys 28, Trp 29, Leu 32, Trp 33 and Phe 36 that lie below the average location of this phospholipid atom (Fig. 2D). This does not occur to such an extent in the POPC-Chol system, where only Phe 36 lies below the POPC P plane and the peptide assumes an orientation more parallel to the membrane surface when completely adsorbed (last 10 ns of the simulation), as is also evident from the tilt angles and in the typical snapshots of Fig. 1D and E.

To get further insight on the driving force behind binding of the peptide to the bilayers, time variations of both short-range Coulomb and Lennard-Jones peptide/lipid and peptide/solvent interaction energies are shown in Fig. 3. Inspection of these plots reveals a lag-time of ~5 ns during which peptide/lipid interaction energy is essentially zero. During this period, the peptide is too distant from the bilayers to "sense" them and diffuses in the water medium. This diffusion eventually leads the peptide to regions in the box where the presence of lipid can be felt. From this point on, both T-20/POPC Coulomb and Lennard-Jones interaction energies decrease gradually (and conversely for the solvation energies). In the early stages of interaction, the two terms have similar magnitude in the POPC system, whereas in the POPC/Chol bilayer the Lennard-Jones contribution is more negative. However, from ~25 ns onwards, the Coulomb term becomes the largest in absolute terms in both systems. This shift probably reflects peptide helix/lipid headgroup reorientation, with concomitant formation of favorable ionic and H-bond interactions. Regarding the POPC/Chol system, it is noteworthy that i) T-20/Chol interaction is negligible; ii) the drop in T-20/POPC interaction energy is clearly lower than in the POPC simulation; and iii) a drop in T-20/POPC energy is observed at ~85 ns, correlating with the changes in peptide orientation and center of mass position commented above.

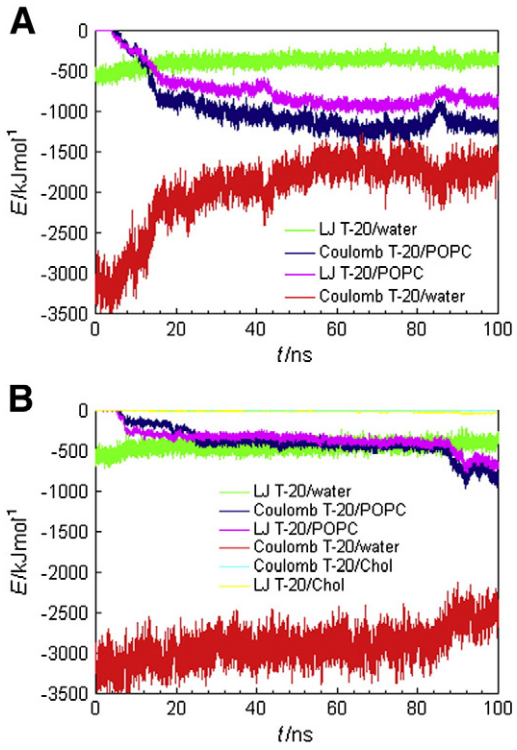

Fig. 3. Time variations of short-range Coulomb and Lennard-Jones peptide/lipid and peptide/solvent interaction energies, in the POPC (A) and POPC/Chol (B) systems.

3.3. Peptide secondary structure

Peptide secondary structure was analyzed with the DSSP program [26]. Percentages of secondary structure features were averaged for the final 25 ns of the simulation (Fig. 4A), and time courses of the secondary structure features were also calculated (Fig. 4B–D). In all systems, T-20 shows a distinct preference for forming a 5′-helix (or π-helix; 60% or more of the overall secondary structure). The helical structure in the membrane is also evident from the profile of the average *Z* coordinate shown in Fig. 2D. It is clear that the residues' positions vary as expected for a helical arrangement, though the period is somewhat larger than the 3.6 residues/turn expected for a strict α-helical structure, and is closer to the 4.1 residues/turn value typical of a π-helix. Generally, there is good agreement between the profile and the theoretical amphipathic profile of the peptide [13], confirming that it is arranged as an amphipathic helix in both membrane systems, located at the water/lipid interface, with mostly hydrophilic residues facing the water medium and conversely for the membrane side.

3.4. Peptide interaction with bilayers — Radial distribution functions (RDF)

Radial distribution functions (RDFs) were calculated between all the T-20 atoms and all the atoms of the phosphate (O7, P8, O9, O10 and O11) and choline (C1, C2, C3 and N4) groups, and, in the POPC/Chol bilayer, also the Chol hydroxyl group (O6 and H7) (Fig. 5A), for the last 25 ns of the simulation time.

The RDFs for the choline group have the highest densities within each system (higher in the POPC system than in the POPC/Chol bilayer in all cases) and the distribution function with the lowest density is the one of T-20 with Chol's hydroxyl group. Although T-20/phosphate RDFs have lower densities than those of the choline (but still higher in the POPC system than in the POPC/Chol bilayer), T-20 appears consistently at a shorter distance from the phosphate group than all the others (≈0.15 nm). This distance and the narrowness of its peak suggest a very specific interaction between certain aminoacid residues of the peptide and the phosphate group.

For further insight, RDFs between individual aminoacid residues and the mentioned lipid polar groups were calculated. Lys28 and Asn34 were found to be the main contributors to the 0.15 nm density peak in the POPC/Chol system (Fig. 5C), whereas in the POPC system the main contributors are Asn14, Gln15, Gln16, Lys18, Asn19, Lys28 and Asn34 (Fig. 5B). These aminoacid residues are all capable of acting as an H donor in an H bond and the distance of the interactions is supportive of such hypothesis.

The fact that the T-20/choline RDF has a very broad peak (in both systems) at ~0.6 nm is probably related to the interfacial location of the choline moiety and its accessibility to the solvent and hence to the peptide itself, rather than to a specific T-20/choline interaction. On the other hand, interaction with the cholesterol hydroxyl group appears to be almost non-existing in comparison. In POPC/Cholesterol mixtures, Chol is expected to be protected from water by the PC headgroup (the so-called umbrella effect [34]). Chol molecules are thus also separated from the peptide and unable to interact with it directly and effectively.

3.5. Peptide interaction with bilayers — H bonds

Following the previous section, formation of H-bonds between individual residues of T-20 (as well the whole peptide) and relevant groups in the bilayer systems was investigated. For this analysis, an H-bond for a given donor–H–acceptor triad was registered each time the donor–acceptor distance was <0.35 nm and the H–donor–acceptor angle was <30°.

Fig. 6 shows the time variation of the number of H-bonds formed between T-20 and the POPC molecules. T-20 is capable of binding to both bilayers via H-bonds and their number increases with time during the 100 ns of the simulation. Adsorption gives rise to a steep increase in the number of H bonds in the POPC system for 10 ns < *t* < 20 ns. On the other hand, the increase in number of T-20/POPC H-bonds is much more gradual in the POPC/Chol bilayer. In the latter, two significant events can be identified from steeper increases: adsorption of the C-terminal region at ~10–30 ns; and adsorption of the whole peptide length at ~80–90 ns (which correlates with the sudden variation of distance between the center of mass of T-20 and the bilayer surface apparent at ~85 ns in Fig. 2C, as well as with the decrease in T-20/POPC interaction energy shown in Fig. 3B). In any case, the number of H bonds in the POPC/Chol system is clearly lower than in the POPC system, and this significant difference cannot solely be explained by the small difference in POPC molecules per leaflet (63 in the POPC bilayer and 60 in the POPC/Chol bilayer).

Individual residues were analyzed (last 25 ns of the simulation) to determine which ones were responsible for the formation of H bonds with the bilayer (Table 1). T-20 interacts via H bonds mainly with the phosphate O atoms and the carbonyl O16 atom. In comparison, interaction with the other POPC ester and carbonyl O atoms is negligible. In the POPC bilayer, the main H bond donor residues are Asn14, Gln15, Gln16, Lys18, Asn19, Lys28 and Asn34 which concurs with the RDFs results. In the POPC/Chol bilayer, only Lys28 and Asn34 contribute significantly to H-bonding to POPC, which also agrees with the RDFs results. Fig. 2D shows that the average positions of each of the residues that act as major H bond donors are closer to the average P z position in the POPC bilayer. This may be one of the causes for the difference in behavior of these residues in the two systems: clearly, the larger distances between most T-20 residues and the P atom plane in POPC/Chol preclude efficient formation of H-bonds. Additionally, in the POPC bilayer, some of the donors appear in clusters: Asn14–Gln15–Gln16 and Lys18–Asn19. This probably stems from the fact that formation of an H-bond between a given residue and phosphate O atoms contributes in turn to approximate and/or provide adequate

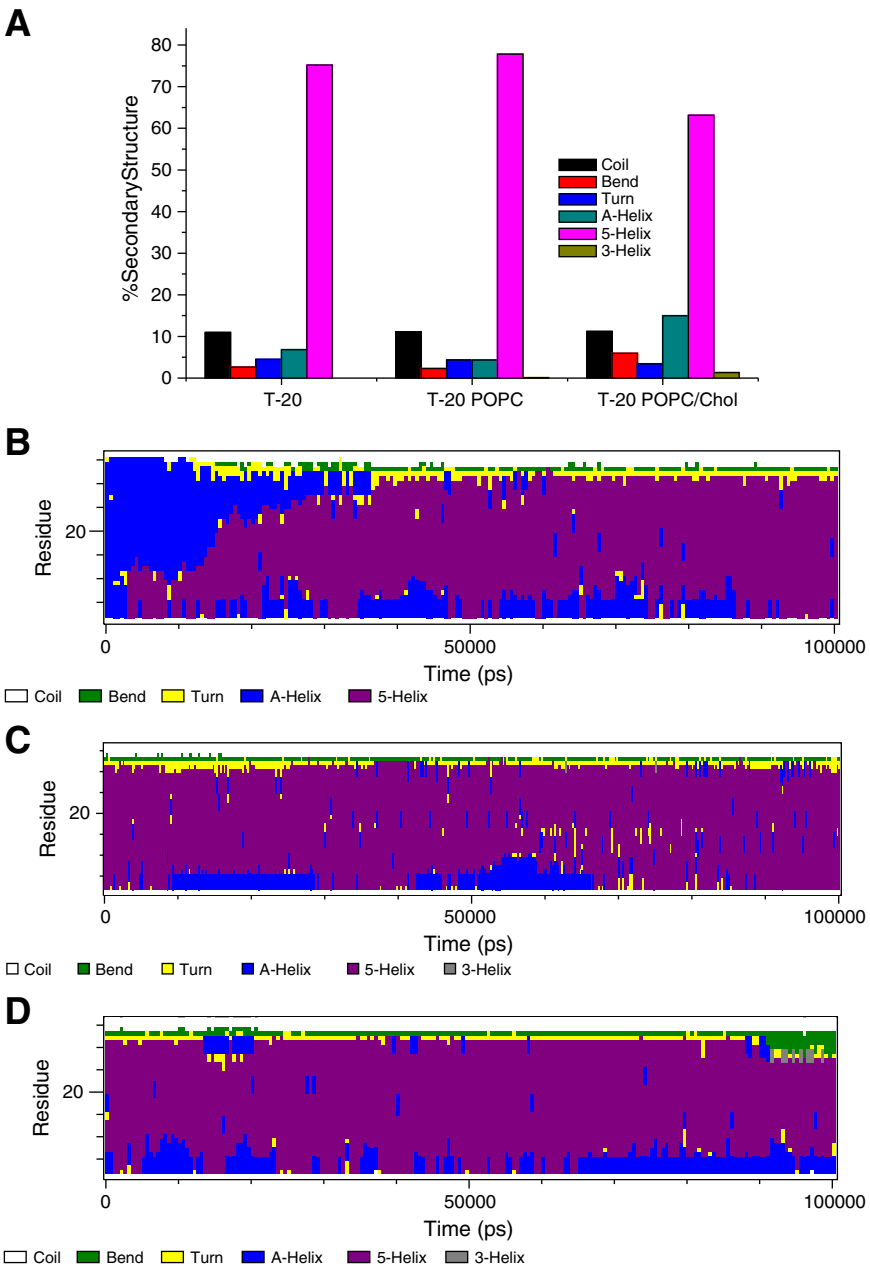

Fig. 4. (A) Average percentages of secondary structure motifs for the last 25 ns of each simulation (error bars represent standard deviation). (B–D) Time courses of secondary structure motifs for the T-20 peptide in the water (B), POPC bilayer (C) and POPC/Chol bilayer (D).

orientation of the neighboring residues relative to the phosphate group, facilitating their own involvement in H-bond formation.

This difference in H-bonding may explain the way the peptide adsorbs differently to the bilayer surfaces: more H bonds in the POPC bilayer, distributed evenly along the peptide helix, allow for a more parallel adsorption, whereas in the POPC + Chol bilayer the H bonds are more restricted to the C-terminus of the peptide for most of the simulation, allowing more freedom of movement to the N-terminus. Only in the later stages of the simulation is parallel adsorption observed.

3.6. Cross-sectional area per lipid and membrane thickness

The cross-sectional area per lipid (POPC or Chol) was calculated as reported in [30] with minor modifications to take into account the volume occupied by the peptide when present. Briefly, both parameters were calculated according to Eqs. (1) and (2). The POPC/Chol bilayers, when compared with the POPC bilayers, showed a lower area per POPC as expected due to the Chol's condensing effect [30,35].

Membrane thickness was determined as the average of the distance between P atoms of different monolayers (P–P distance). Membrane thickness values are difficult to compare to experimental results because a definitive definition of bilayer thickness is still lacking [36]. Overall the POPC/Chol bilayers are thicker than the POPC bilayers, as expected due to the acyl-chain ordering induced by Chol [30,36]. The presence and interaction of the T-20 peptide with the model membranes have the same effect in both cases albeit to different extents: it induces a decrease in the membrane thickness of about 0.8% the POPC membrane and of about 6% in the POPC/Chol membrane (Table 2).

Upon adsorption with the POPC or POPC/Chol bilayers, T-20 induces a decrease in the area per POPC of about 1.9% and 5.8%, respectively (Table 2).

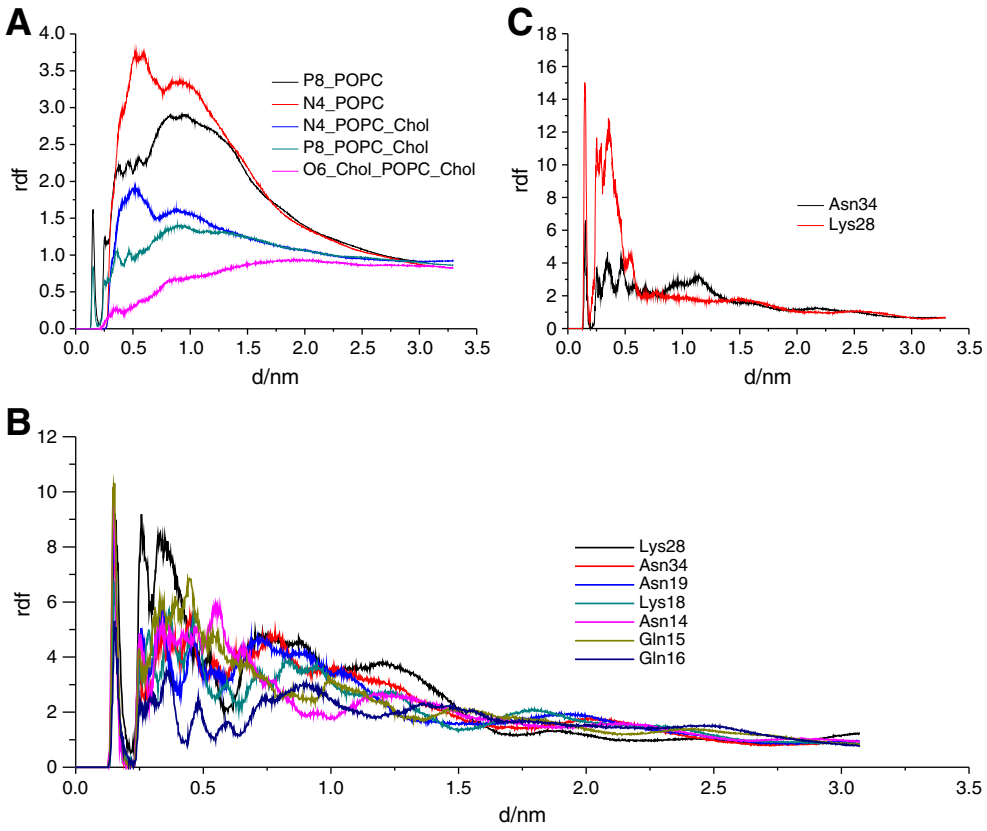

Fig. 5. Radial distribution functions. (A) RDFs between T-20 and the phosphate (P8) and choline (N4) groups in both systems. (B) RDFs between selected aminoacid residues and POPC's phosphate groups in the POPC bilayer. (C) RDFs between selected aminoacid residues and POPC's phosphate groups in the POPC + Chol bilayer.

Contrary to POPC surface area, the area/Chol molecule increases approximately 9% upon T-20 adsorption to the model POPC-Chol membrane (Table 2). This implies that globally the area of the POPC/Chol bilayer is only slightly changed (≈1% decrease) upon adsorption of the peptide. The fact that calculating the average area/POPC and area/Chol using Eqs. (1) and (2) leads to a decrease in the former, and an increase in the latter, should be viewed with caution, because as there is a strong *Z*-dependence between the cross-sectional areas of PC and cholesterol, the average area per phospholipid and area per cholesterol in binary mixtures are in fact poorly defined parameters [35]. The POPC bilayer is a fluid membrane and upon adsorption, T-20 semi-penetrates the membrane surface forming a crater-like burrow around itself as clearly shown in the 2D plot of local bilayer thickness (calculated using the Gridmat-MD program [28]) shown in Fig. 7. This plot represents a 2D map of the bilayer in which the local bilayer thickness is represented across the bilayer plane. Some POPC molecules, the ones directly below the peptide, are pushed toward the bilayer core (Fig. 7). As a result, this compression creates a concavity in the top leaflet that ultimately leads to an average decrease in bilayer thickness, considering the entire bilayer (Table 2).

Profiles of the mass density were calculated for the molecules present in the bilayer systems in study (averaged over the last 25 ns of the simulation) along the normal to the membrane plane as shown in Fig. 8. The compression caused by peptide interaction with the top

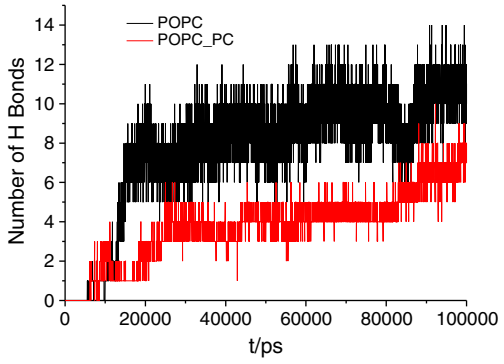

Fig. 6. Time course of the number of H bonds formed between T-20 and POPC molecules in POPC (black) and POPC/Chol (red) bilayers.

Table 1
Average number of H bonds between T-20 (or some relevant aminoacid residues), and relevant atoms in the POPC structure.

	Phosphate O atoms		O16 (carbonyl O atom of *sn*-2 chain)	
	POPC	POPC + Chol	POPC	POPC + Chol
T-20	8.40 ± 1.19	3.93 ± 0.67	1.36 ± 1.26	1.77 ± 0.90
Tyr01	0.13 ± 0.34	0.09 ± 0.28	0.35 ± 0.48	
Thr02		0.00 ± 0.03		
Ser03		0.00 ± 0.06		
His06	0.00 ± 0.04	0.01 ± 0.08		
Gln13	0.00 ± 0.04			
Asn14	1.02 ± 0.14			
Gln15	1.36 ± 0.48		0.55 ± 0.50	
Gln16	0.87 ± 0.34	0.00 ± 0.04		
Lys18	0.90 ± 0.35		0.00 ± 0.02	
Asn19	1.00 ± 0.10		0.46 ± 0.50	
Lys28	1.81 ± 0.65	2.04 ± 0.21		
Trp29	0.21 ± 0.44			
Ser31		0.00 ± 0.03		
Trp33		0.09 ± 0.28		0.36 ± 0.48
Asn34	1.00 ± 0.11	0.68 ± 0.48		1.40 ± 0.51
Trp35		0.03 ± 0.16		

Table 2
Cross-sectional area per lipid in all systems under study and their respective membrane thickness.

	Lipid	Area per lipid /nm^2	Membrane thickness /nm
POPC	POPC	0.645 ± 0.020	3.82 ± 0.13
POPC:CHOL	POPC	0.526 ± 0.017	4.59 ± 0.14
	CHOL	0.252 ± 0.008	
T-20 + POPC	POPC	0.633 ± 0.020	3.79 ± 0.13
T-20 + POPC:CHOL	POPC	0.495 ± 0.016	4.32 ± 0.14
Last 10 ns	CHOL	0.274 ± 0.009	

leaflet is also visible in the POPC density in this region (but not in the cholesterol density). The top leaflet, upon which the peptide adsorbs, consistently has a lower POPC peak density and a slight POPC profile distortion when compared with the bilayers without peptide.

3.7. Order parameters

The order parameter tensor, *S*, is defined as:

$$S_{ab} = \frac{1}{2} < 3\cos(\theta_a)\cos(\theta_b) - \delta_{ab} > \qquad a,b = x,y,z \tag{3}$$

where θ_a (or θ_b) is the angle made by ath (or bth) molecular axis with the bilayer normal and δ_{ab} is the Kronecker delta (<> denotes both ensemble and time averaging). In our simulations using a united atom force field, the order parameter for saturated and unsaturated carbons S_{CD} can be determined using the following relations [37]:

$$-S_{CD}^{Sat} = \frac{2}{3}S_{xx} + \frac{1}{3}S_{yy} \tag{4}$$

$$-S_{CD}^{Unsat} = \frac{1}{4}S_{zz} + \frac{3}{4}S_{yy} + \frac{\sqrt{3}}{2}S_{xy} \tag{5}$$

$-S_{CD}$ may vary between 0.5 (full order along the bilayer normal) and −0.25 (full order along the bilayer plane), whereas $-S_{CD} = 0$ denotes isotropic orientation. Due to the slow convergence of this parameter [38], analysis was restricted to the last 10 ns of the simulations.

$-S_{CD}$ profiles along the *sn*-1 and *sn*-2 chains in POPC, POPC/Chol, T-20/POPC and T-20/POPC/Chol systems are shown in Fig. 9. In the POPC/Chol bilayer, T-20 adsorption generally evokes a decrease in $-S_{CD}$ values in both acyl chain C atoms. In the POPC bilayer the C2–C4 atoms of the *sn*-1 acyl chain suffer a slight increase in $-S_{CD}$, which can be a result of a more local and intense interaction between the bilayer and the peptide, as this effect is not observed in the POPC/Chol bilayer in which peptide adsorption induces chain disordering. In the POPC/Chol bilayer the general effect of peptide adsorption, as stated earlier, is a decrease in $-S_{CD}$ values in both acyl chain C atoms. However, this effect is more pronounced in the *sn*-2 acyl chain's C2–C7 carbons.

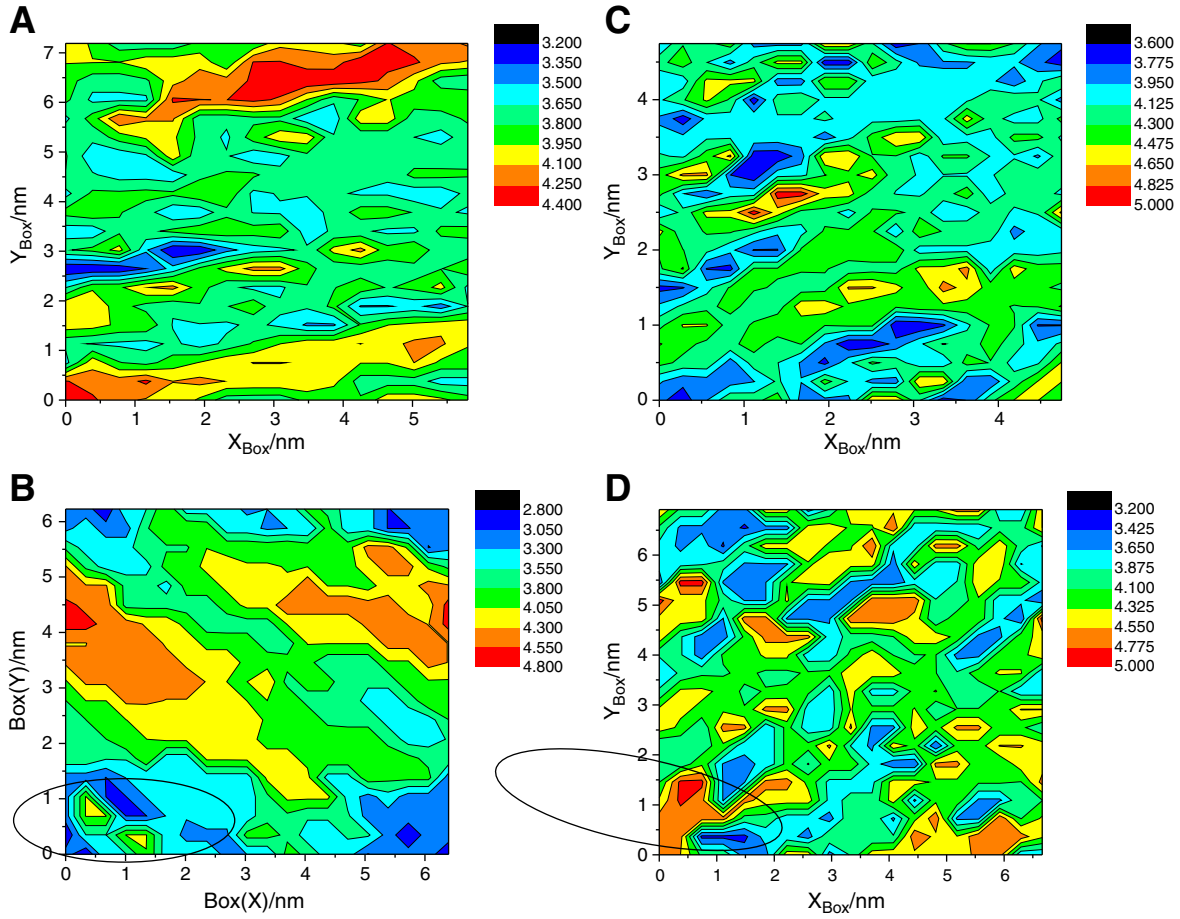

Fig. 7. Membrane thickness contour plot of the last configuration in each system; (A) POPC, (B) T-20 + POPC, (C) POPC/Chol and (D) T-20 + POPC/Chol. Peptide position is depicted as a black ellipse.

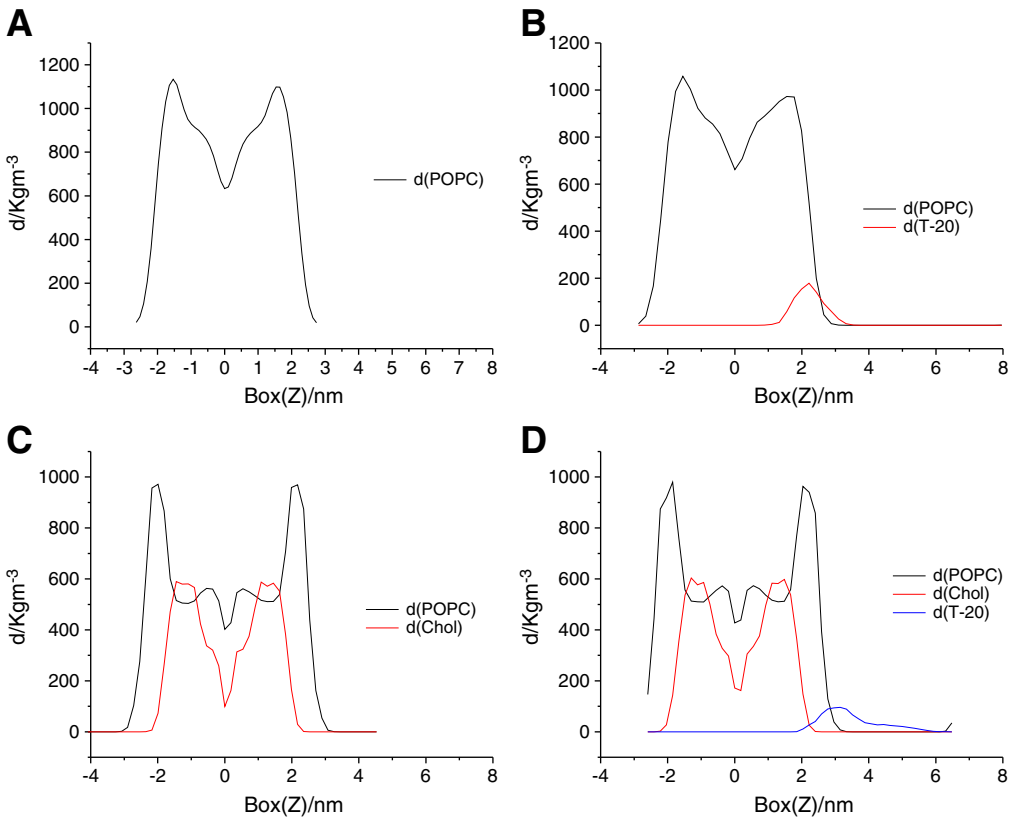

Fig. 8. Mass density profiles. (A) POPC system. (B) POPC/Chol system. (C) T-20/POPC system. (D) T-20/POPC/Chol system.

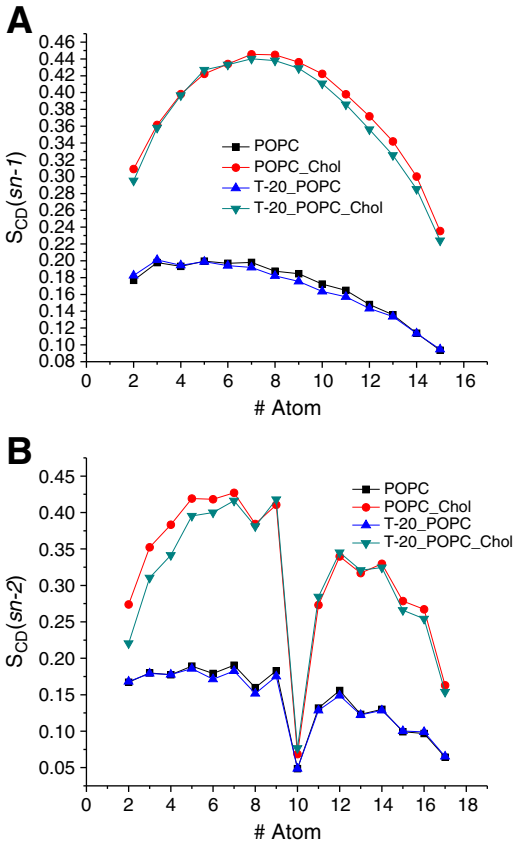

Fig. 9. $-S_{CD}$ order parameters of *sn*-1 (A) and *sn*-2 (B) acyl chains.

3.8. Lateral diffusion of T-20

The diffusion coefficients D of T-20 in water and in contact with bilayers were calculated from the d-dimensional mean square displacement (MSD; $d = 3$ for water, 2 for bilayers) using the Einstein relation:

$$D = \frac{1}{2d} \lim_{t\to\infty} \frac{dMSD(t)}{dt}. \tag{6}$$

In this equation, $MSD(t)$ is defined as:

$$MSD(t) = \left\langle \left\| \vec{R}(t + t_0) - \vec{R}(t_0) \right\| \right\rangle^2 \tag{7}$$

where $\vec{R}$ is the (x,y,z) (for water) or (x,y) (for bilayers) position of the center of mass of the peptide, and the averaging is carried out over time origins t_0. To eliminate noise due to fluctuations in the center of mass of the monolayer that interacts with the peptide, MSD analyses of peptide in contact with bilayers were carried out using trajectories with fixed center of mass of this leaflet [39,40].

Fig. 10A and B shows MSD(t) of T-20 in the studied systems. By fitting Eq. (6) to the linear region of the MSD, $D = (2.98 \pm 0.23) \times 10^{-6}\,\mathrm{cm^2\,s^{-1}}$ was obtained for T-20 in water. This value is close to those calculated for similarly sized peptides in water (e.g., [41]). Additionally, it compares well with the simple estimate from the Stokes–Einstein equation,

$$D = \frac{kT}{6\pi\eta r} = \frac{kT}{6\pi\eta}\left(\frac{4\pi}{3V}\right)^{1/3} \cong \frac{kT}{6\pi\eta}\left(\frac{4\pi}{3(M/N_A)\left(\vec{\nu} + h\right)}\right)^{1/3}. \tag{8}$$

In these equations, k is the Boltzmann constant, T is the absolute temperature, η is viscosity, r and V are the hydrated radius and molar volume (respectively) of the peptide, $M = 4.4921 \times 10^3$ g/mol is the

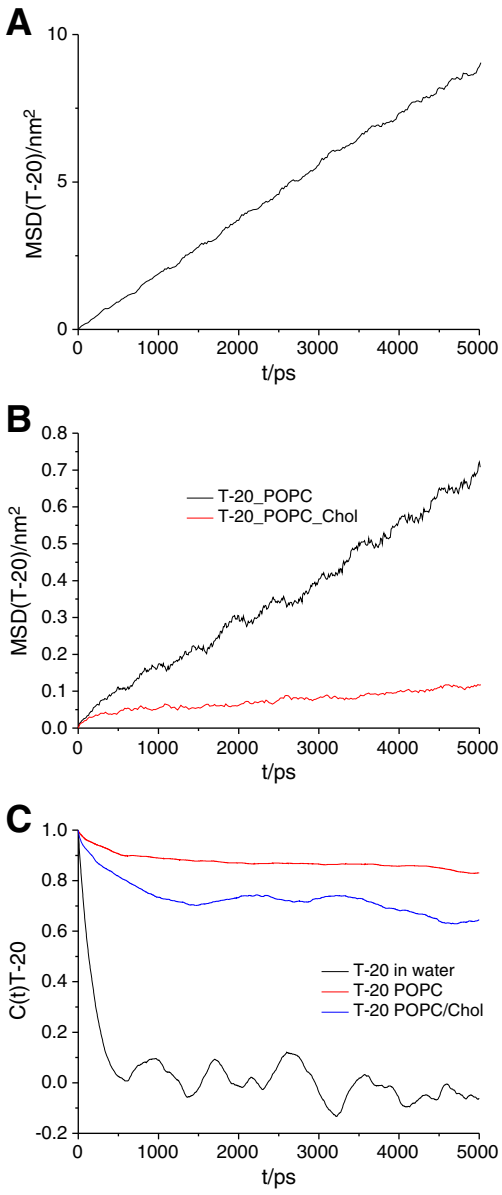

Fig. 10. (A, B) Mean square displacement (MSD) of T-20 in water (A) and lipid bilayers (B). (C) T-20 long axis rotational autocorrelation function for all studied systems.

peptide molar mass, N_A is the Avogadro constant, $\overline{\nu}$ is the protein specific volume and h is the hydration (typical peptide/protein values of 0.73 cm^3/g and 0.23 cm^3/g [42] were used for $\overline{\nu}$ and h, respectively). By substitution, $D = 2.05 \times 10^{-6}\ cm^2\ s^{-1}$ is obtained. The reasonably small discrepancy between the Stokes–Einstein and MD simulation values can be understood by noting that T-20's shape is not spherical (as assumed in Eq. (8)) and SPC water has reduced viscosity relative to H_2O [43].

As shown in Fig. 10B, the peptide moves considerably slower when in contact with the bilayer models than in water, as a result of adsorption. Lateral peptide diffusion is almost an order of magnitude faster in the POPC system ($D_{lat} = (3.37 \pm 0.39) \times 10^{-7}\ cm^2\ s^{-1}$) than in the POPC/Chol bilayer (where $D_{lat} = (3.95 \pm 0.48) \times 10^{-8}\ cm^2\ s^{-1}$). Diffusion of T-20 is less hindered by adsorption to the bilayer systems than T-1249, which showed slower diffusion interacting with POPC and POPC/Chol bilayers [15]. This suggests that T-20 has a lower degree of interaction with the bilayer models and reinforces its lower affinity toward adsorption to POPC/Chol.

3.9. Rotational dynamics of T-20

Rotational dynamics of the T-20 long axis was studied by calculating the rotational auto correlation function $C(t)$ defined below:

$$C(t) = P_2(\cos\theta(\xi)) \tag{9}$$

where $\theta(\xi)$ is the angle between the peptide long axis at times ξ and $t+\xi$, and $P_2(x) = (3x^2 - 1)/2$ is the second order Legendre polynomial. Averaging is performed over ξ, which assuming a sufficiently ergodic trajectory is an approximation of the ensemble average. It should be mentioned that this is a good approximation in water, but probably is not valid in the bilayer systems, where peptide rotation is much more impeded, as described below.

Fig. 10C shows the $C(t)$ functions calculated for the three systems. In water, where the peptide rotates freely, $C(t)$ decays rapidly to zero, and an exponential decay fit to $C(t)$ yields a rotational correlation time of $\theta \approx 1.50$ ns. This value can be compared with the rough estimate obtained using the equation (approximately valid for globular proteins, which is clearly not the case) [42]

$$\theta = \frac{\eta V}{RT} \cong \frac{\eta M}{RT}\left(\vec{\nu} + h\right) \tag{10}$$

where R is the ideal gas constant and other symbols have the same meaning as in Eq. (8). This equation yields $\theta = 1.48$ ns, in excellent agreement with the value obtained from simulation.

In contrast, rotation of the peptide interacting to the bilayer surface is impeded in both bilayer systems, as evident from Fig. 10C. The calculated $C(t)$ functions decrease only 10–30% in the two bilayer systems during the simulation timescale. It is, however, noteworthy that the extent of rotational hindrance is not as severe as that verified for T-1249 ($C(t)$ functions decreased only by 1–3% in the same simulated time [15]), especially for POPC/Chol, and in agreement with the above mentioned experimental data regarding the extent of partition/adsorption to the bilayers.

4. Discussion

POPC and POPC:Chol bilayers represent membranes in two clearly distinct phases, namely the liquid disordered and liquid ordered phases, respectively. 100 ns molecular dynamics simulations of solvated bilayers (POPC and POPC/Chol 1:1) were performed for comparison purposes, as stated earlier. Those bilayers were also analyzed and several parameters where determined both for validation purposes and comparison with the peptide simulations. Our results for the cross-sectional area per POPC (Table 1) agree with the experimental values of 0.65 nm^2 ($T = 298$ K; Lantzsch et al., [44]), 0.64 nm^2 ($T = 298$ K; Konig et al., [45]), and 0.63 nm^2 ($T = 297$ K; Smaby et al., [46]), as well as with those obtained from MD simulations by Böckmann et al. [47] ($T = 300$ K, $a = 0.655\ nm^2$), Mukhopadhyay et al. [48] ($T = 298$ K, $a = 0.62\ nm^2$), Gurtovenko and Anwar [49] ($T = 310$ K, $a = 0.65\ nm^2$), and Pandit et al. [50] ($T = 303$ K, $a = 0.63\ nm^2$). Order parameters were also calculated for both acyl chains of POPC (Fig. 9). The profiles obtained agreed with both experimental (e.g., [51,52]) and simulated (e.g., [47,49,53]) data. Calculated lateral lipid diffusion coefficients (not shown) agreed with values obtained both from NMR experiments [54,55] and MD simulations [47]. Together, these findings validate our bilayer model systems for the study of interaction with T-20.

This study shows that HIV fusion inhibitor peptide T-20 interacts with POPC (liquid disordered phase) and POPC/Chol 1:1 (liquid ordered phase) bilayers, but to a smaller extent than T-1249 [15]. This was verified experimentally by Veiga et al. [13,14]. These authors measured the variation of peptide fluorescence intensity (from the five Trp residues) and determined a lipid/water partition coefficient of

$K_p = (1.6 \pm 0.1) \times 10^3$ in POPC, using a formalism of distribution between aqueous and lipid phases (valid assuming peptide insertion in the bilayer; see below for discussion of the latter hypothesis), significantly lower than that of T-1249 in the same system ($(5.1 \pm 0.7) \times 10^3$). Veiga et al. verified no variation in the peptide's fluorescence parameters upon interaction with POPC/Chol (2:1) liquid ordered bilayers, which could indicate absence of peptide interaction with this bilayer system. These authors discuss the importance of binding to ordered POPC-Chol bilayers as possibly correlating to the increased efficiency of T-1249 relative to other inhibitors such as T-20. The present work shows that, although superficial interaction of T-20 occurs in both POPC and POPC:Chol systems, limited penetration of the C-terminal region occurs only in the former system, whereas in the Chol-rich, ordered phase, the peptide's C-terminal just rests on top of the headgroup region of the bilayer for most of the simulation and only in the last ≈15 ns of the simulation it adopts an almost parallel position on the surface of the bilayer.

This can also explain why it is experimentally verified that there is a measurable change in peptide fluorescence upon interaction with POPC and not so upon interaction with POPC/Chol membranes. Veiga et al. [13,14] hypothesized that absence of T-20 adsorption in the Chol-rich bilayer could leave the Trp fluorescent residues largely exposed to water, and therefore their fluorescence properties would remain unaltered relative to bulk aqueous medium, whereas the peptide would insert in Chol-free bilayers, leading to a measurable increase in Trp emission intensity. Our results agree with this hypothesis in that the three Trp residues (29, 33 and 35) are all in average located above the P atoms of the POPC headgroups in the POPC/Chol system, that is, largely exposed to water. Also in agreement, all three Trp residues have a shallow position in the POPC bilayer, near the water/lipid interface, but clearly deeper than in the POPC/Chol system. In POPC, two of the residues are on average located below the lipid P atoms. This could explain the peptide fluorescence quantum yield increase upon interaction with POPC. However, no effective peptide insertion is observed in the timescale of our simulations, and the peptide stays adsorbed at the interface. This does not necessarily mean that the partition treatment of Veiga et al. and their model of the involvement of lipid membranes in the T-20 mode of action, both of which assume peptide insertion in Chol-free bilayers, are incorrect, because peptide insertion cannot be ruled out for larger timescales, inaccessible to MD simulations. Our simulations show that peptide adsorption is clearly related to the formation of H-bonds between some peptide residues and mainly the POPC phosphate O atoms. The fact that weaker interaction is observed in the POPC/Chol system correlates with the smaller average number of such H bonds in this system. In turn, this is probably due to the reduction in the number of POPC molecules at the expense of Chol, and the fact that the latter is unable to form H-bonds with the peptide because of shielding of the Chol hydroxyl by the phospholipid headgroups (umbrella effect). However, from Fig. 6, it appears that the number of H bonds may still be increasing for both systems near the end of the simulations, supporting further evolution at longer time scales.

This study also indicates that T-20 displays helical conformation both in water and in interaction with membranes. This behavior seems to be important, since it has been recently reported that helix-stabilized HIV-1 fusion inhibitor peptides display high inhibitory efficiency [16]. A non-dominant (8% and 10%) α-helical component was already inferred from circular dichroism (CD) spectra of T-20 in both buffer and POPC [13], respectively. In our study, the predominant structure is 5′-helix (π-helix) (~63–78%), and the α-helix component is reduced to ~4–15% across the three studied systems (Fig. 4). This discrepancy may be caused by different determination methodologies. CD results were treated with the k2d package [56,57] that determines peptide or protein secondary structure from CD spectra using a Kohonen neural network with a 2-dimension output layer and has the limitation of only estimating three general types of secondary structure: the percentages of helix, beta (no differentiation in either case) and all other possible peptide or protein secondary structures. In our MD simulations, secondary structure was determined using the DSSP program [27] that from the atom coordinates determines bond angles and assigns secondary structure motifs based on this unequivocal data. In this view, our results show that the helical structure is, in fact, predominant and is maintained throughout the time scale studied, which implies that this structure is needed for both interaction with the solvent and the membrane.

Regarding T-20's mobility in presence of membranes, it is apparent that both lateral and rotational diffusions are considerably slower than in water (as an obvious consequence of adsorption to the bilayer, Fig. 10). Rotational motion is much more hindered in POPC compared to POPC/Chol (Fig. 10C), which probably reflects the higher number of H-bonds existing between T-20 and POPC in this system. Due to the large energy penalty associated with breaking H-bonds, together with the highly directional character of these interactions (implying that they cease to be operative upon peptide rotation), it is very clear that the larger the number of T-20/lipid H bonds, the more impeded is the peptide's rotation. On the other hand, lateral diffusion shows the reverse trend, being considerably slower in POPC/Chol (Fig. 10B). This apparently contradictory finding can be explained taking into account that, due to the peptide adsorption to POPC headgroups by means of persistent H bonds, most lateral motion of the peptide is actually due to that of the POPC lipids underneath, which is faster in the liquid disordered POPC bilayer than in the liquid ordered POPC/Chol system. Finally, both rotation and lateral diffusion of T-20 are significantly less impeded than those of the similar peptide inhibitor T-1249 [15], which is a probable consequence of the stronger membrane interaction of the latter.

5. Concluding remarks

In sum, despite the obvious limitations concerning the sampling timescale (which precluded the study of slower interaction processes, such as eventual peptide insertion) and simulation of a single peptide molecule (with obvious consequences in terms of statistics; a possible way to circumvent this would be averaging over a number of shorter simulations with different initial structures), our simulations provide detailed insight on the nature of the interaction of T-20 with model membranes, indicating that the peptide adsorbs (with less affinity than T-1249) to the surface of both POPC and POPC/Chol 1:1 bilayers (weakly in the latter case), without insertion in the studied timescale. A defined amphipathic helical structure is observed, which has been related in the literature to increased efficiency in HIV fusion inhibition. The peptide diffuses in the plane of the bilayer (accompanying the host POPC molecules to which it is bound) and possesses some rotational freedom, higher in the POPC/Chol system. T-20 is able to establish H-bonds with POPC but not with Chol, and therefore the number of H-bonds is higher in the pure POPC system, which could explain the peptide's higher affinity to this bilayer system. These observations mostly agree with the model of Veiga et al. [13] for the role of lipid bilayers in the mode of action of the peptide and may explain the relative poor action of the peptide against HIV fusion when compared with other similar, more recently developed peptides [13–15] since low affinity to the bilayers implies low local concentrations of the peptide and the bilayer surface is thus unable to act efficiently as a reservoir for the anti-fusion peptide.

Acknowledgments

The authors acknowledge funding by FEDER, through the COMPETE program, and by FCT, project reference FCOMP-01-0124-FEDER-010787 (FCT PTDC/QUI-QUI/098198/2008), and thank Dr. Miguel A. Avillez for access to computing facilities.

References

[1] P.M. Colman, M.C. Lawrence, The structural biology of type I viral membrane fusion, Nat. Rev. Mol. Cell Biol. 4 (2003) 309–319.
[2] M.K. Lawless, S. Barney, K.I. Guthrie, T.B. Bucy, S.R. Petteway, G. Merutka, HIV-1 membrane fusion mechanism: Structural studies of the interactions between biologically-active peptides from gp41, Biochemistry 35 (1996) 13697–13708.
[3] L.A. Lasky, G. Nakamura, D.H. Smith, C. Fennie, C. Shimasaki, E. Patzer, P. Berman, T. Gregory, D.J. Capon, Delineation of a region of the human immunodeficiency virus type 1 gp120 glycoprotein critical for interaction with the CD4 receptor, Cell 50 (1987) 975–985.
[4] T. Dragic, V. Litwin, G.P. Allaway, S.R. Martin, Y. Huang, K.A. Nagashima, C. Cayanan, P.J. Maddon, R.A. Koup, J.P. Moore, W.A. Paxton, HIV-1 entry into CD4+ cells is mediated by the chemokine receptor CC-CKR-5, Nature 381 (1996) 667–673.
[5] S. Jiang, Q. Zhao, A.K. Debnath, Peptide and non-peptide HIV fusion inhibitors, Curr. Pharm. Des. 8 (2002) 563–580.
[6] T. Matthews, M. Salgo, M. Greenberg, J. Chung, R. DeMasi, D. Bolognesi, Enfuvirtide: the first therapy to inhibit the entry of HIV-1 into host CD4 lymphocytes, Nat. Rev. Drug Discov. 3 (2004) 215–225.
[7] C.T. Wild, D.C. Shugars, T.K. Greenwell, C.B. McDanal, T.J. Matthews, Peptides corresponding to a predictive alpha-helical domain of human immunodeficiency virus type 1 gp41 are potent inhibitors of virus infection, Proc Natl. Acad. Sci. U. S. A. 91 (1994) 9770–9774.
[8] C.E. Baldwin, R.W. Sanders, B. Berkhout, Inhibiting HIV-1 entry with fusion inhibitors, Curr. Med. Chem. 10 (2003) 1633–1642.
[9] L.A. Cooley, S.R. Lewin, HIV-1 cell entry and advances in viral entry inhibitor therapy, J. Clin. Virol. 26 (2003) 121–132.
[10] J.M. Kilby, J.J. Eron, Novel therapies based on mechanisms of HIV-1 cell entry, N. Engl. J. Med. 348 (2003) 2228–2238.
[11] J.J. Eron, R.M. Gulick, J.A. Bartlett, T. Merigan, R. Arduino, J.M. Kilby, B. Yangco, A. Diers, C. Drobnes, R. DeMasi, M. Greenberg, T. Melby, C. Raskino, P. Rusnak, Y. Zhang, R. Spence, G.D. Miralles, Short-term safety and antiretroviral activity of T-1249, a second-generation fusion inhibitor of HIV, J. Infect. Dis. 189 (2004) 1075–1083.
[12] R.M. Gulick, New antiretroviral drugs, Clin. Microbiol. Infect. 9 (2003) 186–193.
[13] A.S. Veiga, N.C. Santos, L.M. Loura, A. Fedorov, M.A. Castanho, HIV fusion inhibitor peptide T-1249 is able to insert or adsorb to lipidic bilayers. Putative correlation with improved efficiency, J. Am. Chem. Soc. 126 (2004) 14758–14763.
[14] S. Veiga, S. Henriques, N.C. Santos, M. Castanho, Putative role of membranes in the HIV fusion inhibitor enfuvirtide mode of action at the molecular level, Biochem. J. 377 (2004) 107–110.
[15] A.M.T.M. do Canto, A.J.P. Carvalho, J.P.P. Ramalho, L.M.S. Loura, Structure and conformation of HIV fusion inhibitor peptide T-1249 in presence of model membranes. A molecular dynamics study, J. Mol. Struct. Thoechem 946 (2010) 119–124.
[16] P.M. Matos, M.A.R.B. Castanho, N.C. Santos, HIV-1 fusion inhibitor peptides enfuvirtide and T-1249 interact with erythrocyte and lymphocyte membranes, PLOS One 5 (2010) e9830.
[17] M.A. Thompson, ArgusLab 4.0.1, Planaria Software LLC, Seattle, WA, 2004.
[18] H.J.C. Berendsen, J.P.M. Postma, W.F.v. Gunsteren, J. Hermans, Interaction models for water in relation to protein hydration, in: B. Pullman (Ed.), Intermolecular Forces, D. Models Publishing Company, Dordrecht, 1981, pp. 331–342.
[19] M. Holtje, T. Forster, B. Brandt, T. Engels, W. von Rybinski, H.D. Holtje, Molecular dynamics simulations of stratum corneum lipid models: fatty acids and cholesterol, BBA-Biomembr. 1511 (2001) 156–167.
[20] H. Bekker, H.J.C. Berendsen, E.J. Dijkstra, S. Achterop, R.v. Drunen, D.v.d. Spoel, A. Sijbers, H. Keegstra, B. Reitsma, M.K.R. Renardus, GROMACS: a parallel computer for molecular dynamics simulations, in: R.A.d. Groot, J. Nadrchal (Eds.), Physics Computing, 92, World Scientific, Singapore, 1993.
[21] D. Van der Spoel, E. Lindahl, B. Hess, G. Groenhof, A.E. Mark, H.J.C. Berendsen, GROMACS: fast, flexible, and free, J. Comput. Chem. 26 (2005) 1701–1718.
[22] H.J.C. Berendsen, J.P.M. Postma, W.F. Vangunsteren, A. Dinola, J.R. Haak, Molecular-dynamics with coupling to an external bath, J. Chem. Phys. 81 (1984) 3684–3690.
[23] S. Miyamoto, P.A. Kollman, Settle — an analytical version of the shake and rattle algorithm for rigid water models, J. Comput. Chem. 13 (1992) 952–962.
[24] B. Hess, H. Bekker, H.J.C. Berendsen, J.G.E.M. Fraaije, LINCS: a linear constraint solver for molecular simulations, J. Comput. Chem. 18 (1997) 1463–1472.
[25] K.A. Feenstra, B. Hess, H.J.C. Berendsen, Improving efficiency of large time-scale molecular dynamics simulations of hydrogen-rich systems, J. Comput. Chem. 20 (1999) 786–798.
[26] U. Essmann, L. Perera, M.L. Berkowitz, T. Darden, H. Lee, L.G. Pedersen, A smooth particle mesh Ewald method, J. Chem. Phys. 103 (1995) 8577–8593.
[27] W. Kabsch, C. Sander, Dictionary of protein secondary structure — pattern-recognition of hydrogen-bonded and geometrical features, Biopolymers 22 (1983) 2577–2637.
[28] W.J. Allen, J.A. Lemkul, D.R. Bevan, GridMAT-MD: a grid-based membrane analysis tool for use with molecular dynamics, J. Comput. Chem. 30 (2009) 1952–1958.
[29] H. Flyvbjerg, H.G. Petersen, Error estimates on averages of correlated data, J. Chem. Phys. 91 (1989) 461–466.
[30] C. Hofsass, E. Lindahl, O. Edholm, Molecular dynamics simulations of phospholipid bilayers with cholesterol, Biophys. J. 84 (2003) 2192–2206.
[31] S. Oishi, S. Ito, H. Nishikawa, K. Watanabe, M. Tanaka, H. Ohno, K. Izumi, Y. Sakagami, E. Kodama, M. Matsuoka, N. Fujii, Design of a novel HIV-1 fusion inhibitor that displays a minimal interface for binding affinity, J. Med. Chem. 51 (2008) 388–391.
[32] H. Nishikawa, S. Oishi, M. Fujita, K. Watanabe, R. Tokiwa, H. Ohno, E. Kodama, K. Izumi, K. Kajiwara, T. Naitoh, M. Matsuoka, A. Otaka, N. Fujii, Identification of minimal sequence for HIV-1 fusion inhibitors, Bioorg. Med. Chem. 16 (2008) 9184–9187.
[33] H. Nishikawa, S. Nakamura, E. Kodama, S. Ito, K. Kajiwara, K. Izumi, Y. Sakagami, S. Oishi, T. Ohkubo, Y. Kobayashi, A. Otaka, N. Fujii, M. Matsuoka, Electrostatically constrained alpha-helical peptide inhibits replication of HIV-1 resistant to enfuvirtide, Int. J. Biochem. Cell Biol. 41 (2009) 891–899.
[34] J. Dai, M. Alwarawrah, J. Huang, Instability of cholesterol clusters in lipid bilayers and the cholesterol's Umbrella effect, J. Phys. Chem. B 114 (2010) 840–848.
[35] M. Alwarawrah, J.A. Dai, J.Y. Huang, A molecular view of the cholesterol condensing effect in DOPC lipid bilayers, J. Phys. Chem. B 114 (2010) 7516–7523.
[36] T. Rog, M. Pasenkiewicz-Gierula, Cholesterol effects on a mixed-chain phosphatidylcholine bilayer: a molecular dynamics simulation study, Biochimie 88 (2006) 449–460.
[37] S.A. Pandit, E. Jakobsson, H.L. Scott, Simulation of the early stages of nano-domain formation in mixed bilayers of sphingomyelin, cholesterol, and dioleylphosphatidylcholine, Biophys. J. 87 (2004) 3312–3322.
[38] L.M.S. Loura, J.P.P. Ramalho, Location and dynamics of acyl chain NBD-labeled phosphatidylcholine (NBD-PC) in DPPC bilayers. A molecular dynamics and time-resolved fluorescence anisotropy study, BBA-Biomembr. 1768 (2007) 467–478.
[39] C. Anezo, A.H. de Vries, H.D. Holtje, D.P. Tieleman, S.J. Marrink, Methodological issues in lipid bilayer simulations, J. Phys. Chem. B 107 (2003) 9424–9433.
[40] E. Lindahl, O. Edholm, Molecular dynamics simulation of NMR relaxation rates and slow dynamics in lipid bilayers, J. Chem. Phys. 115 (2001) 4938–4950.
[41] R.P. Bora, R. Prabhakar, Translational, rotational and internal dynamics of amyloid β-peptides (Aβ40 and Aβ42) from molecular dynamics simulations, J. Chem. Phys. 131 (2009) 155103.
[42] J.R. Lakowicz, Principles of Fluorescence Spectroscopy, 2nd Edition Kluwer/Plenum Press, Dordrecht/New York, 1999.
[43] P.E. Smith, W.F. van Gunsteren, The viscosity of SPC and SPC/E water at 277 K and 300 K, Chem. Phys. Lett. 215 (1993) 315–318.
[44] G. Lantzsch, H. Binder, H. Heerklotz, M. Wendling, G. Klose, Surface areas and packing constraints in POPC/C(12)EO(n) membranes. A time-resolved fluorescence study, Biophys. Chem. 58 (1996) 289–302.
[45] B. Konig, U. Dietrich, G. Klose, Hydration and structural properties of mixed lipid/surfactant model membranes, Langmuir 13 (1997) 525–532.
[46] J.M. Smaby, M.M. Momsen, H.L. Brockman, R.E. Brown, Phosphatidylcholine acyl unsaturation modulates the decrease in interfacial elasticity induced by cholesterol, Biophys. J. 73 (1997) 1492–1505.
[47] R.A. Bockmann, A. Hac, T. Heimburg, H. Grubmuller, Effect of sodium chloride on a lipid bilayer, Biophys. J. 85 (2003) 1647–1655.
[48] P. Mukhopadhyay, H.J. Vogel, D.P. Tieleman, Distribution of pentachlorophenol in phospholipid bilayers: a molecular dynamics study, Biophys. J. 86 (2004) 337–345.
[49] A.A. Gurtovenko, J. Anwar, Interaction of ethanol with biological membranes: the formation of non-bilayer structures within the membrane interior and their significance, J. Phys. Chem. B 113 (2009) 1983–1992.
[50] S.A. Pandit, S.W. Chiu, E. Jakobsson, A. Grama, H.L. Scott, Cholesterol packing around lipids with saturated and unsaturated chains: a simulation study, Langmuir 24 (2008) 6858–6865.
[51] J. Seelig, N. Waespesarcevic, Molecular order in cis and trans unsaturated phospholipid bilayers, Biochemistry-Us 17 (1978) 3310–3315.
[52] G. Klose, B. Madler, H. Schafer, K.P. Schneider, Structural characterization of POPC, and C12E4 in their mixed membranes at reduced hydration by solid state H-2 NMR, J. Phys. Chem. B 103 (1999) 3022–3029.
[53] M. Patra, E. Salonen, E. Terama, I. Vattulainen, R. Faller, B.W. Lee, J. Holopainen, M. Karttunen, Under the influence of alcohol: the effect of ethanol and methanol on lipid bilayers, Biophys. J. 90 (2006) 1121–1135.
[54] T. Kochy, T.M. Bayerl, Lateral diffusion-coefficients of phospholipids in spherical bilayers on a solid support measured by H-2-nuclear-magnetic-resonance relaxation, Phys. Rev. E 47 (1993) 2109–2116.
[55] W. Febo-Ayala, D.P. Holland, S.A. Bradley, D.H. Thompson, Lateral diffusion coefficients of an eicosanyl-based bisglycerophosphocholine determined by PFG-NMR and FRAP, Langmuir 23 (2007) 6276–6280.
[56] M.A. Andrade, P. Chacon, J.J. Merelo, F. Moran, Evaluation of secondary structure of proteins from UV circular-dichroism spectra using an unsupervised learning neural-network, Protein Eng. 6 (1993) 383–390.
[57] J.J. Merelo, M.A. Andrade, A. Prieto, F. Moran, Proteinotopic feature maps, Neurocomputing 6 (1994) 443–454.